ZANCO Journal of Pure and Applied Sciences

TYPE Original article
DOI http://dx.doi.org/10.21271/ZJPAS.37.1.12

OPEN ACCESS

*Corresponding author
Basil Younus Mustafa
basil.mustafa@epu.edu.iq

RECEIVED :01 /08 /2024
ACCEPTED :28/12/ 2024
PUBLISHED :28/ 02/ 2025

KEYWORDS:
Flood Hazard Index (FHI), GIS spatial analysis, Digital Elevation Model (DEM), Analysis Hierarchy Process (AHP), Flood Hazard Map, Sensitivity Analysis, Nature-based Solutions (NABs).

Flash Flood Hazard Mapping Using Analytical Hierarchy Process (AHP) and GIS Application: In the Barzan Area of Iraqi Kurdistan Region

Basil Younus Mustafa[1], Mohammed Dler Faisal[2], DE WILDE Roeland[3], Ali R. Ahmed[4] ,Mohamed Moafak Arbili[5],

1 Civil Engineering Department, Technical Engineering College, Erbil Polytechnic University, Erbil, Kurdistan Region, Iraq.
2 Information Management Officer (IOM) - Erbil Polytechnic University, Erbil, Kurdistan Region, Iraq .
3 IMO Head, Preparedness and Response Division, IOM Iraq.
4 Presidency of Erbil Provincial Council.
5 Civil Engineering Department, Technical Engineering College, Erbil Polytechnic University, Erbil, Kurdistan Region, Iraq.

ABSTRACT

Addressing the combined hazards of flooding and water scarcity in the same region requires a large-scale, evidence-based approach to disaster risk reduction. This investigation presents the evaluation of flood hazard area on a large scale for flood-prone Barzan region as a multi-criteria index, located 80 km northeast of Erbil City-Iraqi Kurdistan Region. The Flood Hazard Index (FHI) is delimited, and GIS spatial analysis is utilized to predict its value. The methodology, integrates information from ten parameters: Topographic of Wetness Index (TWI), Elevation (E), Slope (S), Precipitation (P), Land Use Land Cover (LULC), Normalized Difference Vegetation Index (NDVI), Distance from River (D_1), Distance from Road (D_2), Density of Drainage (D_3), with type of Soil (S). The importance of each characterizes in flood amount and severity is reflected through weight values calculated utilizing the Analyzing Hierarchy Process (AHP). Flood hazard mapping is generated by superimposing information from the parameters based on their weight values. The generated flood hazard map for the area under study, classifying flood vulnerability into five categories: very low, low, moderate, high, and very high. The generated flood hazard map for the study area indicates that regions with very high and high flood susceptibility are predominantly located in the central, southeastern, and southwestern parts, with a smaller area in the northwest. The distribution of the area across different flood susceptibility levels is as follows: 14% falls into the very high category, 24% into the high category, 23% into the moderate category, 25% into the low category, and 14% into the very low category. Areas with very high flood vulnerability are primarily situated near rivers, particularly the Greater Zab and Rezan Rivers. The method's accuracy is validated through sensitivity analysis, exploring various weight values and alternative scenarios. The sensitivity analysis leads to a revised index FHIS and flood mapping, reaffirming the methodology's robustness. Comparison with historical flood actions confirms the validity of the proposed approach. The methodology therefore suggests itself as a basis for large-scale predictive flood hazard mapping. The parameters of this approach also suggest it as a potential basis for planning Nature-based Solutions (NABs) on a large geographic scale.

1.Introduction

Flooding hazards are the result of water exceeding the limits of its habitual seasonal location, affecting floodplains and posing risks to residents, livestock, crops, and wildlife.

The standard approach to flood hazards involves two components: flood risk assessment and mitigation, acknowledging that complete risk elimination is neither feasible nor efficient. Large-scale strategies, for example for a region within a country, or at the national level, require identifying areas at risk, enabling early warning systems, swift responses, and ultimately reducing the effect of possible flood actions (Kazakis et al., 2015).

Floods have emerged as the greatest collective natural hazard in recent decades , with its frequency of severe impact increasing annually due to factors like climate change, urbanization, population growth, construction covering watercourses, and ill-suited rainwater drainage channels (Rahmati et al., 2016, Ushiyama et al., 2017, Green et al., 2000).

Flood hazard diagramming is essential for efficient and effective land use planning in flood-prone regions. It provides easily understandable and quickly available graphs and charts, authorities to categorize areas at hazard and arrange justification and response effort. Mapping floods and assessing their risk in different areas requires considering several influences (Poussin et al., 2014, Ali and Mawlood, 2023b, Muhammad et al., 2023).

GIS is a powerful appliance to recognize flood-prone areas, playing a crucial role in planning and implementing strategies to mitigate the impact of this natural hazard to protect lives, properties, livelihoods and resources, including biodiversity (Correia et al., 1999). Using GIS systematically on a larger scale increases the effectiveness of mitigation measures by covering larger networks of catchment areas (Gigović et al., 2017).

In several research projects multicriteria decision analysis (MCDA) techniques have proven effective, and are accepted as crucial tools for addressing complex decision problems. Multicriteria decision analysis integrates a range of conditions, including methodological, eco-friendly, and socioeconomic influences (Liu et al., 2003), intending to accomplish optimal resolution-production (Ghanbarpour et al., 2013). This process establishes reference environments to classify overflow hazard areas (Yang et al., 2011). While combined with a (GIS) system, MCDA maps inundation zones. GIS techniques enhance the management and investigation of altitudinal data, simplifying the conception, analysis, and estimation of MCDA consequences (Wang et al., 2011).

Saaty et al. (2012) introduced the Analytical Hierarchy Process (AHP) as a mathematical approach employed for multi-standards resolution-production (Lawal et al., 2014). The method follows Saaty's importance value scale, assigning arithmetic values ranging from 1 to 9 to factors based on their relative significance. A value of 1 denotes equal importance, whereas 9 indicates a significant difference in significance, in accordance with (Saaty et al.) established methodology (Table 1).

AHP has proven effective in several requests such as flood predisposition mapping, especially in groundwater and landslide mapping, as well as within chemical fields (Kaliraj et al., 2014, Razandi et al., 2015, Althuwaynee et al., 2014, Hanratty and Joseph, 1992, Pirdashti et al., 2009). This technique assigns weight values to assess the significance of factors. Using these weights, the (FHI) can be computed to determine the probability of flooding (Elkhrachy, 2015). The Flood Hazard Index Sensitivity (FHIS) is then identified to examine the sensitivity of pairwise comparisons to changes in criteria weights, proving effective in situations with uncertainty about the importance of each factor (Yahaya, 2008, Ali and Mawlood, 2023a).

In a provincial-measure research, Kazakis et al. (2015) developed a (FHI) to assess flood-prone areas. Using altitudinal investigation in a GIS environment, the investigations included seven factors, such as flow increase, detachment from the sewer system, altitude, land-dwelling usage, precipitation amount, and geology. AHP was utilized to conclude weight values for each factor, and these weights were applied to create flood hazard diagrams in a flood-prone area in

northeastern Greece.

Rahmati et al. (2016) evaluated the use of the AHP to classify probable flood hazard areas, paralleling consequences with a hydraulic model. Firstly, considering four characters detachment to the river, land use, elevation, and land slope along the Yasooj River in Iran, normalized weights were determined using Saaty's nine-point scale. The criteria were combined utilizing a weighted linear combination method in ArcGIS 10.2, which was then utilized to build a flood hazard prediction map.

Gigović et al. (2017) established a consistent GIS software in urban area, as multi-conditions procedure for mapping flood risk areas. This approach integrates GIS with multi-conditions decision analysis (MCDA) by considering six key factors: elevation, slope, distance to the sewer network, distance from the water surface, water level, and land use. The methodology is tested using three AHP-based scenarios namely the Interlude Approximate Numbers Approach (IR'AHP), the Fuzzy Technique (F'AHP), and the outmoded AHP (Fair) method. This procedure has been applied in Palelula Municipality, Belgrade, Serbia, where it creates an urban flood risk map that agrees well with historical flood data, with the IR'AHP procedure showing the maximum level of agreement.

Hammami et al. (2019) instructed a spatial multi-criteria resolution-making pattern to measure flooding susceptibility in Tunis. Eight criteria were carefully analyzed and integrated into ArcGIS to identify hazardous zones. The AHP was used for flood hazard modelling, considering the bulk and overgrown of each criterion. This process computed the FHI, consequential in a flood predisposition map categorized from low to high-class flood potential.

Swain et al. (2020) used a multi-criteria resolution sustenance system to revision a flood-prone region in Bihar, India, combining AHP with GIS/remote sensing technologies using the Google Earth Instrument (GEI) platform. The research measured five key flood-causing criteria, each subdivided into 21 sub-criteria. The comparative significance of criteria was resolute through the AHP pair-wise assessment matrix (PCM), highlighting hydrologic and anthropogenic interference as the most and least significant factors, respectively. About 40.36% of the analyzed area fell within high to high flood susceptibility areas, primarily near rivers, while 12% exhibited very low susceptibility.

Okorafor et al. (2021) employed GIS techniques to identify highly flood-prone areas in Imo State, Southeastern Nigeria. Using satellite imagery and SRTM data, they utilized ArcGIS 10.2 and Global Mapper v15 to create flood maps, and numerical elevation models (NEMs), and conduct flood vulnerability assessments, the investigation identified both the most and least flood-prone areas.

This study assesses flood hazard areas on a large scale in the flood-prone Barzan region using a multi-criteria index approach. The FHI is delimited, and GIS spatial analysis is utilized to estimate its value. The methodology integrates data from ten parameters, assigning weight values based on their significance in flood magnitude and severity, as determined through the AHP. Flood hazard mapping for the study area is then produced by overlaying the parameter data according to their weight values.

Table (1): Saaty scale (1980)

Scale	Numerical rating	Reciprocal
Extremely importance	9	1/9
Very to extremely strongly importance	8	1/8
Very strongly importance	7	1/7
Strongly to very strongly importance	6	1/6
Strongly importance	5	1/5
Moderately to strongly importance	4	1/4
Moderately importance	3	1/3
Equally to moderately importance	2	1/2
Equally importance	1	1

2. Methods and Materials section

2.1 The area under study

The study area for this article is Barzan, 80 km northeast of Erbil City as demonstrated in fig. (1), near the town Barzan, between UTM system

coordinates north (409031, 4107457), south (436089, 4050794), east (440745, 4064541), and west (395283, 4096474). The study area contains 11 catchments whose areas were higher than 8.8 km^2 (Fig. 2). This zone comprises two zones, Barzan to the west and, to the east, Gali Balnda (Nature_Iraq, 2007)

The study area has been suggested as a possible national park. It features the Rezan River and the Shanidar Cave, known for Neanderthal burial sites, rocky gorges and towering cliffs, and oak forests. The area extends north, the Turkish border, and to the south, the Greater Zab River . (Nature_Iraq, 2007, 2009)

Gali Balnda is a basin through which the Deraluk River flows, flanked by mountains, to the Greater Zab River. The ecological characteristics of Gali Balnda resemble those of the primary Barzan region, as both are in the Zagros Range; however, Gali Balnda's geological composition is marked by sandstone, clay, and gravel (Nature_Iraq, 2007).

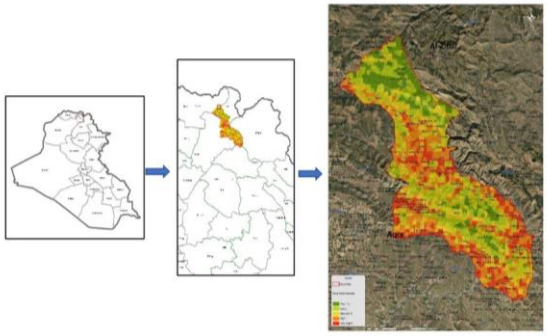

Fig. (1): The location of study area (Barzan)

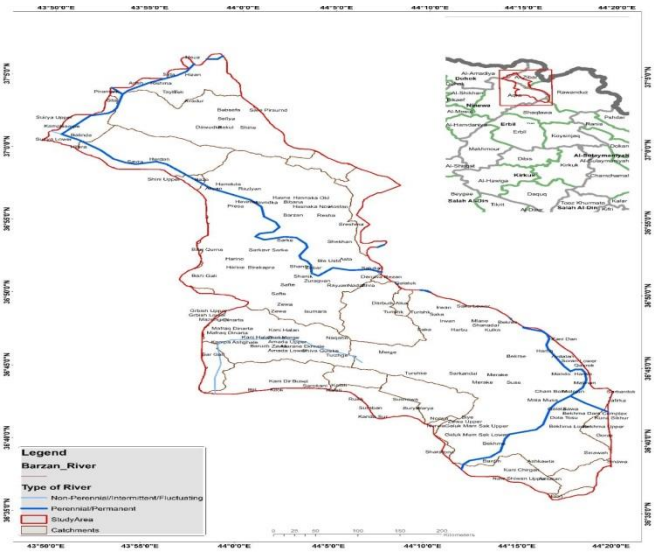

Fig. (2): The study area (Barzan)

2.2 Flood Hazard Index (FHI)

This study presents, a GIS-based index model created to delineate flood hazard areas. The model incorporates a Flood Hazard Index (FHI) through a multi-criteria analysis in which the FHI pinpoint flood risk hotspots and enables a relative assessment across dissimilar basins. The suggested procedure is shown in Fig. (3) (Siddayao et al., 2014).

Remote sensing was employed to extract key spatial parameters that were crucial for the flood hazard mapping process. These include:

1- Land Use and Land Cover (LULC) Mapping: Sentinel-2 satellite imagery with 10-meter resolution was used to classify various land cover types within the study area. A supervised classification method generated thematic maps of different LULC categories, including rangeland, agricultural areas, and urban regions. These maps provided crucial insights into how land cover types affect surface runoff and infiltration, significantly influencing flood hazard susceptibility (Handbook and Tools, 2015).

2- Normalized Difference Vegetation Index (NDVI): NDVI was calculated from Sentinel-2 imagery to evaluate vegetation health and density. Highlighting areas with varying vegetation levels. Denser vegetation, represented by higher NDVI values, promotes water retention and infiltration, helping to reduce flood risk. In contrast, lower values indicate sparse vegetation, increasing runoff potential (Handbook and Tools, 2015).

3- Elevation and Slope Data: Elevation and slope data were derived from the Shuttle Radar Topography Mission (SRTM) Digital Elevation Model (DEM) with a 30-meter resolution. The Slope tool in ArcGIS Desktop was applied to the DEM to accurately calculate slope values across the study area. This analysis was critical for modeling the topography, understanding surface water flow patterns, and identifying areas prone to water accumulation (Farr et al., 2007, ArcGIS, 2010).

4- Drainage and Stream Network Delineation: Remote sensing was also used to delineate stream networks and drainage density in the study area. DEM data, combined with GIS-based hydrological tools, was used to generate flow

direction and accumulation layers, facilitating the extraction of stream channels and the calculation of drainage density. This drainage density map was key to assessing the landscape's ability to manage surface runoff, contributing to flood hazard evaluation.

Finally, data from several sources are input into the GIS. In the second phase, this information is processed, and, in conjunction with the determination of parameter weights, produces the FHI index (Malczewski, 2006). The historical flood event records validate the methodology's accuracy.

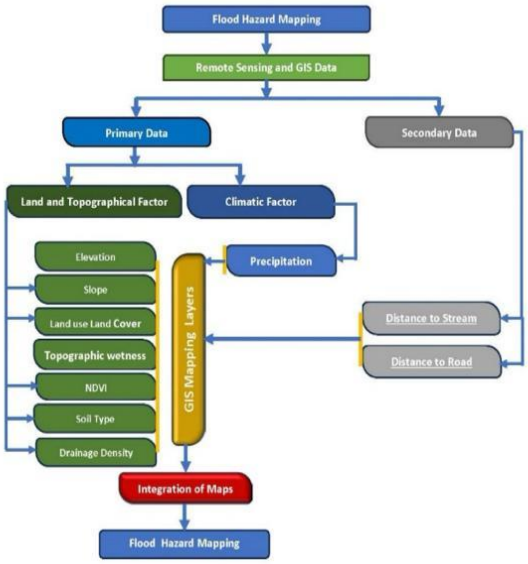

Fig. (3): Conceptual model based on analytical hierarchy process (AHP) for flood hazard mapping by GIS

2.3Factors integrated into the Flood Hazard Index (FHI)

The Flood Hazard Index (FHI) encompasses ten criteria parameters: Topographic Wetness Index (TWI) (T), Elevation (E), Slope (S), Precipitation (P), Land Use Land Cover (LULC) (L), Normalized Difference Vegetation Index (NDVI) (N), Distance from River (D_1), Distance from Road (D_2), Drainage Density (D_3), and Soil Type (S). The collection of these factors is theoretically grounded in their relevance to flood hazards, and have demonstrated effectiveness in previous research studies and applications (Wang and Xie, 2018). In a GIS environment, input data for each parameter undergoes processing, and the ten characterizes are presented in autonomous thematic diagrams. TWI (T), Elevation (E), Slope (S), and Density of Drainage (D_3) are generated from the numerical elevation model (NEM). Geographical evidence provides insights into geological units, while land utilize information finding in the suitable thematic diagram. The detachment from rivers is considered by establishing safeguard areas round drainage network information (Chorley and Kennedy, 1971). To conclude, rainfall intensity is estimated based on rainfall capacities.

The method considers the parameters above, with the weight assigned to each factor influencing its contribution to the outcome. Consequently, a spatial analysis of the study area assesses each grid point based on each factor. Subsequently, local conditions assign values on a scale to each grid point following (Kazakis et al., 2015).

$$FHI = \sum_{i=1}^{n} r_i * w_i \quad \ldots\ldots\ldots\ldots (1)$$

Where: r_i is the represented the rating of the factor in each point, w_i is the weight assigned to each parameter, and n denoted the total number of the criteria.

In flood risk management, the Topographic Wetness Index (TWI) parameter is a crucial analytical tool that provides insights into the spatial variation of soil moisture, indicating the susceptibility of an area to flooding. TWI is a numerical indicator derived from terrain analysis, that quantifies the propensity of a given area to retain surface water, influenced by local topography. TWI is calculated using the following formula (Moore et al., 1991):

$$TWI = \ln\left(\frac{A}{\tan(\beta)}\right) \quad \ldots\ldots\ldots\ldots\ldots (2)$$

Where A signifies the upstream catchment area contributing to water flow at a point, and tan(β) represents the slope gradient at that point. This logarithmic ratio reflects the equilibrium between catchment size and slope, where higher TWI values suggest areas more susceptible to saturation and, thus, potential flooding.

The Land Use and NDVI values were derived from the near-infrared (NIR) and red bands (Red) of Sentinel-2 imagery taken in May 2023, to evaluate vegetation health during the peak growing season. Ranging from -0.34 to 0.47, the NDVI values offered a clear representation of

vegetative cover and its impact on flood risk. The imagery underwent preprocessing to account for atmospheric disturbances, and the NDVI was calculated using the standard formula (Rouse et al., 1974):

$$\mathrm{NDVI} = \frac{(\mathrm{NIR}-\mathrm{Red})}{(\mathrm{NIR}+\mathrm{Red})} \quad \ldots\ldots\ldots\ldots\ldots (3)$$

Slope data was obtained from the Shuttle Radar Topography Mission (SRTM) Digital Elevation Model (DEM) with a 30-meter resolution. This dataset was chosen for its high accuracy and suitability for analyzing topographic features in large areas like Barzan. The slope was calculated using the ArcGIS Spatial Analyst tool, enabling a continuous evaluation of topographical steepness across the study area.

This study emphasizes the historical importance of rainfall in flood events within the study area, as it plays a crucial role in flood risk assessment. In this study, 11-year average annual rainfall data for the study area were analyzed, and obtained from the Global Climate Comprehensive Dataset (https://worldclim.org/).

Stream and drainage density extraction were delineated from the Digital Elevation Model (DEM), using the Hydrology toolset in ArcGIS. Flow direction and flow accumulation layers were first generated to identify stream channels based on threshold values appropriate for the hydrology of the study area. Drainage density was calculated by dividing the total length of streams by the unit area (measured in meters per square kilometer). The Strahler stream ordering method was applied to classify stream segments, producing a detailed drainage density map, which was validated using topographic maps and field observations.

2.3 Analytical Hierarchy Process (AHP)

Through the AHP was established to the weight of collectively factor. AHP is a structured procedure employed for investigating involved problems that entail a collection of consistent objectives or criteria. The criteria are weighted based on the important by determined by the ranking. After hierarchically sorting all criteria, a pairwise assessment matrix is established for each criterion, facilitating an expressive comparison. The comparative significance between criteria is assessed on a scale from 1 to 9, representing less to much more significant standards, correspondingly. The assessment of criteria implication through pairwise investigation yielded the principal eigenvalues defined in Table (2).

Table (3) presents the normalized values of the parameters from Table (2), their mean, and ultimately the corresponding weight (w) assigned to each factor.

Table (2): Parameters of flood hazard: Analytical Hierarchy Process

Parameters	TWI	Elevation	Slope	Precipitation	LULC	NDVI	Distance from river	Distance from road	Drainage density	Soil type
TWI	1	3	2	7	4	2	6	2	5	3
Elevation	1/3	1	1	5	2	2	4	1	3	2
Slope	1/2	1	1	5	3	3	4	1	2	3
Precipitation	1/7	1/5	1/5	1	2	2	4	1	3	3
LULC	1/4	1/2	1/3	1/2	1	1	4	1	3	2
NDVI	1/2	1/2	1/3	1/2	1	1	5	1	3	2
Distance from river	1/6	1/4	1/4	1/4	1/4	1/5	1	1	2	3
Distance from road	1/2	1	1	1	1	1	1	1	2	3
Drainage density	1/5	1/3	1/2	1/3	1/3	1/3	1/2	1/2	1	1
Soil type	1/3	1/2	1/3	1/3	1/2	1/2	1/3	1/3	1	1

Table (3): Normalized flood hazard parameters: Analytical Hierarchy Process

Parameters	TWI	Elevation	Slope	Precipitation	LULC	NDVI	Distance from river	Distance from road	Drainage density	Soil type	Weights	Weights %
TWI	0.255	0.362	0.288	0.335	0.265	0.153	0.201	0.203	0.200	0.130	0.239	24%
Elevation	0.084	0.121	0.144	0.239	0.133	0.153	0.134	0.102	0.120	0.087	0.132	13%
Slope	0.128	0.121	0.144	0.239	0.199	0.230	0.134	0.102	0.080	0.130	0.151	15%
Precipitation	0.036	0.024	0.029	0.048	0.133	0.153	0.134	0.102	0.120	0.130	0.091	9%
LULC	0.064	0.060	0.048	0.024	0.066	0.077	0.134	0.102	0.120	0.087	0.078	8%
NDVI	0.128	0.060	0.048	0.024	0.066	0.077	0.168	0.102	0.120	0.087	0.088	9%
Distance from river	0.043	0.030	0.036	0.012	0.017	0.015	0.034	0.102	0.080	0.130	0.050	5%
Distance from road	0.128	0.121	0.144	0.048	0.066	0.077	0.034	0.102	0.080	0.130	0.093	9%
Drainage density	0.051	0.040	0.072	0.016	0.022	0.025	0.017	0.051	0.040	0.043	0.038	4%
Soil type	0.084	0.060	0.048	0.016	0.033	0.038	0.011	0.034	0.040	0.043	0.041	4%

2.4 Consistency Check Assessment

The steps for computing the Consistency Index (CI), as well as the Consistency Ratio (CR) derived from the pairwise assessment conditions, can be clarified as surveys:

The Consistency Index (CI) is computed to scale the level of consistency in decisions compared to large samples of purely random judgments. Its formula is expressed as (Saaty, 1977):

$$\mathrm{CI} = \frac{\lambda \mathrm{max} - \mathrm{n}}{\mathrm{n}-1} \qquad \ldots\ldots\ldots\ldots (4)$$

Where: $\lambda \mathrm{max}$ is the principal eigenvalue of the pairwise comparison matrix. n is the number of parameters in the matrix. In this investigation, the computation of λ_{max} involved multiplying each column of the pairwise comparison matrix by the corresponding priority vector (weight) and summing these products across all parameters. This sum was then divided by the sum of the priority vector to obtain λ_{max}. With the number of parameters denoted as n (equal to 10 in this case), the calculated λ_{max} was 11.233. Subsequently, equation (2) for the Consistency Index (CI) was applied, resulting in a CI value of 0.137.

The Consistency Ratio (CR) is calculated to determine the acceptability of the consistency index (Saaty, 1977), comparing it against a random index (RI) that represents an index of consistency from a randomly generated matrix. The CR formula is:

$$\mathrm{CR} = \frac{\mathrm{CI}}{\mathrm{RI}} \qquad \ldots\ldots\ldots\ldots (5)$$

Whereas: RI represents the Random Consistency Index, a value contingent upon the number of parameters. Table (4) provides tabulated values of the Random Index (RI) according to Gigović et al. (2017), which vary based on the number of parameters. In this investigation, the number of parameters is set at 10, and from Table (4), RI equals 1.49.

By utilizing the computed (CI) and applying equation (3), the Consistency Ratio (CR) was determined, resulting in a value of 0.092. According to the theory of the AHP, it is recommended that the Consistency Ratio (CR) be less than 0.1. Since CR's value is lower than the threshold (0.1) the weights' consistency is affirmed, (Saaty et al., 2012).

Table (4): Random index (RI)

N	1	2	3	4	5	6	7	8	9	10
Random index (RI)	0	0	0.58	0.9	1.12	1.24	1.32	1.41	1.45	1.49

3.1.1 Results and Discussion

3.1.2 Description Flood Hazard Index Parameters:

3.1.3 Topographic Wetness Index

In Fig. (4a) and table (5), the Topographic Wetness Index (TWI) analysis reveals notable variation in terrain wetness, spanning from 0.81 to 24.

Additionally, Fig. (4b) demonstrates the reclassification of TWI into five flood susceptibility classes, ranging from very high to very low. Lower TWI values indicate well-drained areas with steeper slopes, posing lower flood risks. Higher TWI values, especially 17 km² (about 2% of the study area) in the very high category, and 51 km² (approximately 6%) in the high category, signal potential flood-prone zones. These areas require focused flood risk management, suggesting measures like green infrastructure or improved drainage systems to mitigate the risk and impact of flooding events.

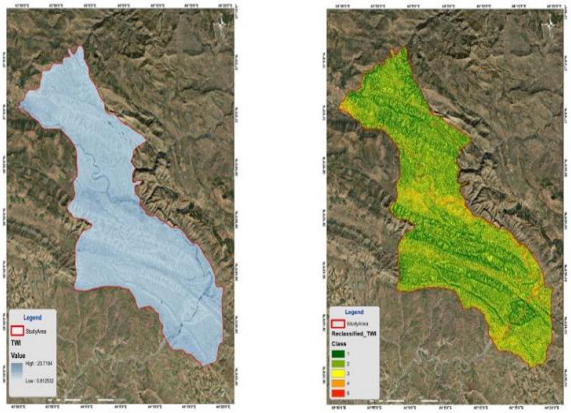

Fig. (4): Thematic map of the TWI parameter in the study area

3.1.4 Elevation

Elevation plays a crucial role in flood risk management, influencing water flow, flood patterns, and runoff sources. It is essential for modeling and preventing floods, with high-resolution elevation data, such as LiDAR, enhancing model accuracy and risk assessment. The elevation analysis in Fig. (5a) reveals a diverse topography within the study area, ranging from 388 to 2309 meters. About 33.44% of the terrain is classified as flat, with minimal elevation variance (Table 5). These flat areas, especially at lower elevations, pose increased flood risk due to water accumulation and reduced runoff efficiency. Identifying and assessing these flat areas is crucial for effective flood risk management and the development of targeted mitigation strategies.

Additionally, Fig. (5b) demonstrates the reclassification of elevation into five flood susceptibility classes, ranging from very high to very low.

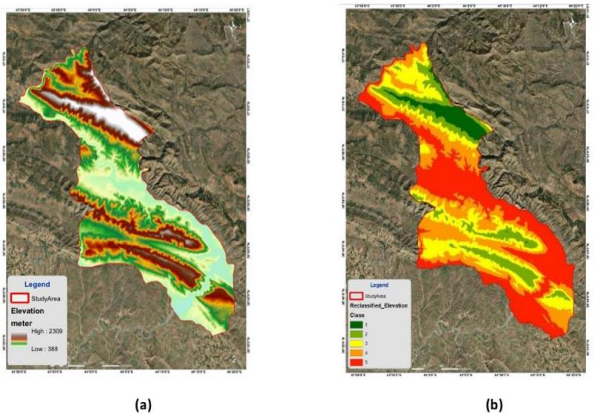

Fig. (5): Thematic map of the Elevation parameter in the study area

3.1.5 Slope

For the flood risk management, the slope is crucial. Steep slopes increase runoff and flood risk, while gentle slopes enhance infiltration and reduce flooding. Accurate slope analysis aids in designing flood defenses and stormwater systems and is vital for land use planning to maintain natural water flow and minimize flood vulnerability. The elevation analysis within the study area as illustrated in Fig. (6a) presents a range from a low of 388 meters to a high of 2,309 meters, signifying considerable topographic diversity. A notable 33% of the study area, covering 304 km², falls into the low elevation category (Table 5), which is significant for flood risk management considerations. This low-lying terrain, particularly the flat areas with minimal elevation variance, is inherently prone to flooding due to potential water accumulation and less efficient runoff. Additionally, Fig. (6b) demonstrates the reclassification of slope into five flood susceptibility classes, ranging from very high to very low.

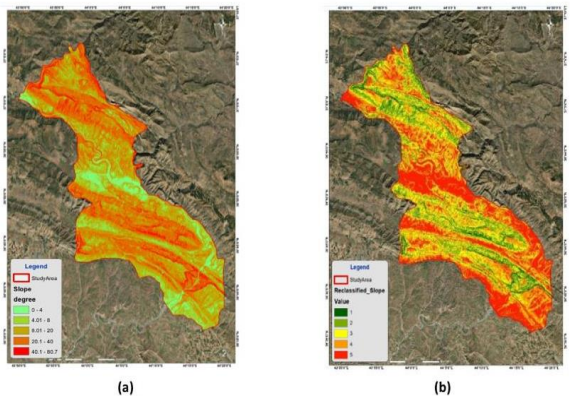

Fig. (6): Thematic map of the Slope parameter in the study area

Table (5): Parameter categories and their corresponding weights

#	Flood Causative Criterion	Unit	Class	Susceptibility Class Ranges and Ratings	Susceptibility Class Ratings	Weight (%)
1	Topographic Wetness Index (TWI)	Level	0.81 - 4.9	Very Low	1	24%
			5 - 6.5	Low	2	
			6.6 - 8.8	Moderate	3	
			8.9 - 12	High	4	
			13 - 24	Very High	5	
2	Elevation	m	390 - 690	Very High	5	13%
			700 - 960	High	4	
			970 - 1,300	Moderate	3	
			1,400 - 1,700	Low	2	
			1,800 - 2,300	Very Low	1	
3	Slope	%	0 - 4	Very High	5	15%
			4.01 - 8	High	4	
			8.01 - 20	Moderate	3	
			20.1 - 40	Low	2	
			40.1 - 80.7	Very Low	1	
4	Precipitation	mm/year	595 - 690	Very Low	1	9%
			690 - 785	Low	2	
			785 - 880	Moderate	3	
			880 - 975	High	4	
			975 - 1070	Very High	5	
5	LULC	Level	Water body	Very High	5	8%
			Crops	High	4	
			Built-up area	Moderate	3	
			Bare ground	Low	2	
			Tree, Rangeland	Very Low	1	
6	NDVI	Level	(-0.343) – (-0.0277)	Very High	5	9%
			(-0.0276) – (0.136)	High	4	
			(0.137) – (0.191)	Moderate	3	
			(0.192) – (0.259)	Low	2	
			(0.26) – (0.477)	Very Low	1	
7	Distance from River	m	0 - 110	Very High	5	5%
			120 - 230	High	4	
			240 - 340	Moderate	3	
			350 - 460	Low	2	
			470 - 570	Very Low	1	
8	Distance from Road	m	0 - 40	Very High	5	9%
			40 - 110	High	4	
			120 - 180	Moderate	3	
			190 - 270	Low	2	
			280- 520	Very Low	1	
9	Drainage density	m/Km	0.361 - 1.73	Very Low	1	4%
			1.74 - 3.11	Low	2	
			3.12 - 4.48	Moderate	3	
			4.49 - 5.85	High	4	
			5.86 - 7.22	Very High	5	
10	Soil Type	Level	Loam	Low	2	4%

3.1.6 Precipitation

Precipitation strongly impacts flood dynamics, influenced by intensity, duration, and spatial distribution. Intense rainfall can surpass the land's absorption capacity, causing increased runoff and potential flooding. Soil conditions, particularly saturated or frozen soils, amplify runoff. Accurate precipitation data is vital for hydrological models to predict floods and technologies like Doppler radar support real-time forecasting. The precipitation analysis within the study area as illustrated in Fig. (7a), the very high precipitation category (975 to 1070 mm) covers about 255 km^2, which is approximately 28% of the investigated area. In addition, the high precipitation category (880 to 975 mm) covers an area of approximately 253 km^2, which constitutes another 28% of the investigated area (Table 5). These designations highlight regions highly susceptible to flooding, emphasizing the necessity for targeted flood mitigation and adaptive management strategies. Additionally, Fig. (7b) demonstrates the reclassification of precipitation into five flood susceptibility classes, ranging from very high to very low.

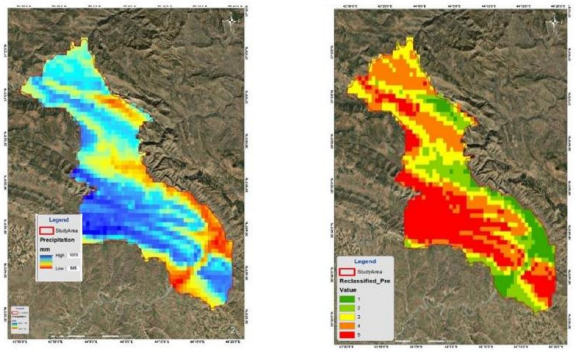

Fig. (7): Thematic map of the Precipitation parameter in the study area

3.1.7 Land Use land Cover (LULC)

In flood risk management, Land utilize and Land Cover (LULC) delineation is crucial due to its significant impact on hydrological systems. Urbanization increases impervious surfaces, intensifying surface runoff and the risk of urban flooding. Conversely, natural terrains like forests and wetlands, as well as areas applying regenerative agriculture, promote the water infiltration and retention that are crucial for flood abatement. Evaluating LULC's influence on flood dynamics is vital for developing nuanced flood mitigation strategies. Using Sentinel-2 outpost imagery for Land Use and Land Cover (LULC)

classification, the analysis of the study area's LULC map as illustrated in Table (6) and (Fig. 8a) reveals a landscape predominantly characterized by rangeland, covering 798.97 km² or 88% of the study area. This dominant land cover significantly influences regional hydrological behavior, impacting flood patterns. Although urbanized zones constitute a smaller footprint (28.54 km² or 3% of the investigation domain), their impervious nature poses a significant flood risk by increasing runoff. Agricultural expanses (52.45 km² or 6%) and forested regions (16.40 km² or 2%) which is enhances water infiltration and storage. Additionally, Fig. (8b) demonstrates the reclassification of (LULC) into five flood susceptibility classes, ranging from very high to very low.

Table (6): Land Use and Land Cover in the study area

LAND USE LAND COVER	Area (km²)	PERCENTAGE
Bare Ground	1.9	0.21 %
Built-up area	27.6	3.05 %
Crops	50.1	5.53 %
Rangeland	798.9	88.14 %
Tree	16.4	1.80 %
Water body	11.5	1.27 %
Total Area	906.5	100 %

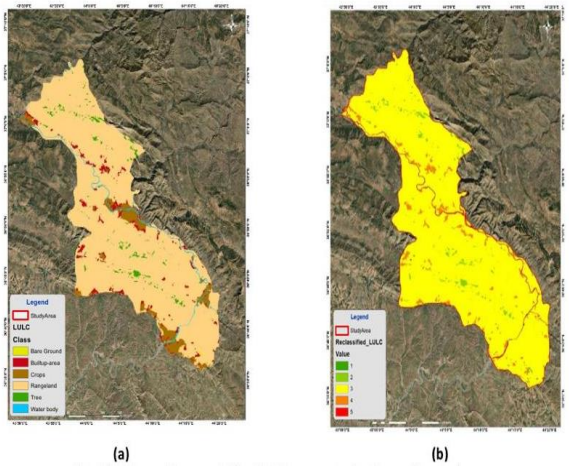

Fig. (8): Thematic map of the (LULC) parameter in the study area

3.1.8 Normalized Difference Vegetation Index (NDVI)

NDVI values in the study area as shown in (Fig. 9a) and Table (5) range from (-0.342969) to (0.477301), offering a comprehensive representation of vegetated and non-vegetated surfaces. Higher values near the upper limit indicate healthier and denser vegetation. In flood risk administration, NDVI plays a key role in illustrating the relationship between vegetation health and hydrological processes like infiltration, evapotranspiration, and surface runoff. Higher NDVI values in regions indicate healthier vegetation cover, leading to enhanced water infiltration and retention, thereby reducing flood risk. Conversely, the interstation zone reveals that around 17% of the land (around 150 km²) exhibits lower NDVI values, representing sparse or unhealthy vegetation, making these areas more susceptible to increased runoff and heightened flood risks. Additionally, Fig. (9b) demonstrates the reclassification of (NDVI) into five flood susceptibility classes, ranging from very high to very low.

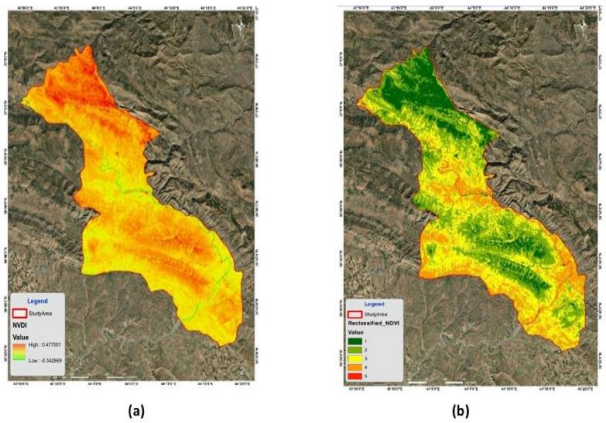

Fig. (9): Thematic map of the (NVDI) parameter in the study area

3.1.9 Distance to road

In flood risk management, the 'Distance to road' metric shows a vital role in water runoff and flow. Areas closer to roads often experience increased flood risks due to the impervious nature of road surfaces, limiting water infiltration and enhancing runoff. Additionally, roads can act as barriers redirecting water flow, contributing to localized flooding.

In Fig. (10a) and Fig. (10b), the outcomes and reclassification of 'distance to road' are showcased into five flood susceptibility classes, spanning from very high to very low, respectively. Regions near roads exhibit elevated flood hazards. Approximately 427 km² or 47% of the study area falls within the 'very high danger' zone

for flooding, notably associated with the proximity to roads. This underscores the crucial need for integrated flood management approaches to tackle challenges arising from urban infrastructure.

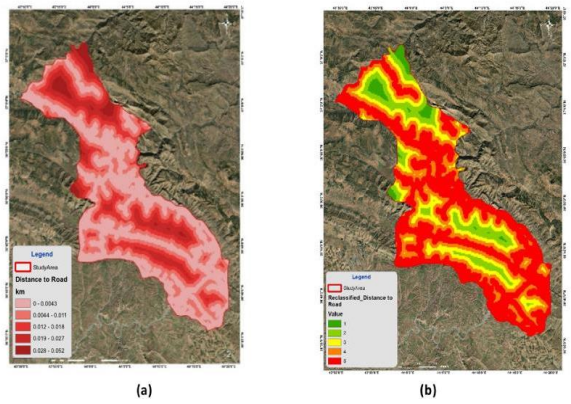

Fig. (10): Thematic map of the 'Distance to road parameter in the study area

3.1.10 Distance to Stream

The 'Distance to stream' is pivotal in flood risk assessment due to the elevated risk near streams and rivers. Proximity to these water bodies makes areas susceptible to flooding, especially during heavy rainfall. Strategic management of floodplains and infrastructure development with flood-resilient measures is crucial to ensure safe distances from watercourses. The investigation zone has been considered based on the distance from streams using satellite imagery analysis (Fig. 11a). Five distinct classes were identified, with the immediate zone adjacent to streams (0 - 110 m) labeled as having a high flood hazard. The risk decreases progressively with increased distances. Areas within the closest proximity to the stream (<110 m) are of particular concern, necessitating enhanced flood protection and prevention strategies. Conversely, regions situated at greater distances (>460 m) from the stream network experience reduced impacts from flooding, highlighting the importance of this parameter in spatial flood risk modeling and infrastructure planning. (Fig.11b) illustrates the NDVI reclassification, dividing the study area into five flood sensitivity categories, from high to very little range.

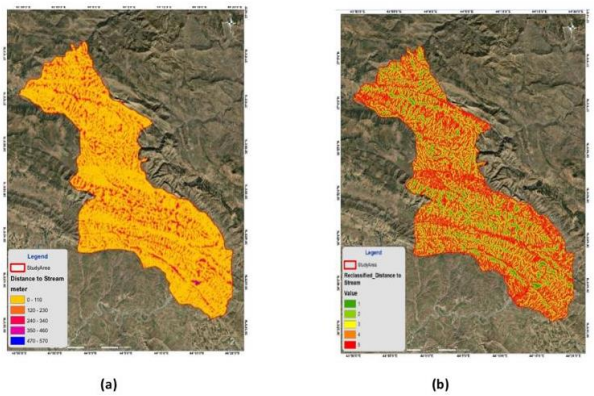

Fig. (11): Thematic map of the Distance to Stream parameter in the study area

3.1.10 Drainage Density

Drainage concentration, representing the total length of watercourses and rivers per unit area, is crucial in assessing flood risk. It reflects the potential for water flow in a watershed, where high drainage density often corresponds to improved surface runoff and a more risk of flooding. This metric shows a key role in guiding watershed management and shaping targeted flood mitigation and drainage management strategies, including NBS methods like swales diverting water that accumulates upstream from weirs or dams made from loose rocks without mortar or cement, or gabion baskets.

When delineating drainage density in the study area (Fig. 12a), the metric has been classified into measurable classes. The category of very high drainage density, ranging from 5.86 to 7.22 m/km, encompasses approximately 88 km², constituting 10% of the study area. The high drainage density class, with values from 4.49 to 5.85 m/km, spans approximately 218 km², representing 24% of the study area. Together, these classifications cover 34% of the study area, indicating regions with heightened flood risk. Additionally, (Fig. 12b) demonstrates the reclassification of drainage density into five flood susceptibility classes, ranging from very high to very low.

These findings emphasize the importance of considering drainage capacity in these areas, requiring the implementation of NBS infrastructure and land management practices to mitigate the risk of adverse hydrological impacts.

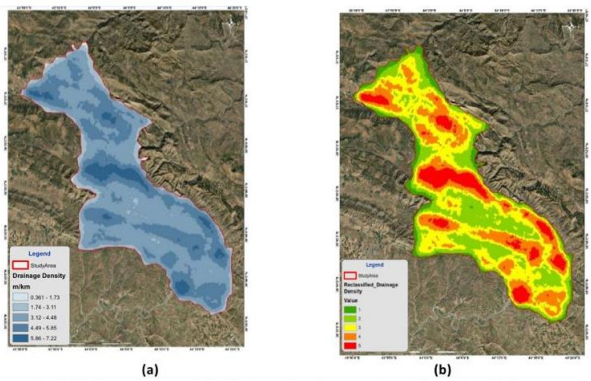

Fig. (12): Thematic map of the drainage density parameter in the study area

3.1.11 Soil Type

Soil type significantly influences flood risk management by impacting water infiltration and retention. In our investigation, soil types were delineated using a GIS layer, revealing that medium-textured soils predominate in the study area as shown in (Fig. 13a), known for balanced infiltration and water-holding capacities. This comprehensive soil and topographical data, from the Food and Agriculture Organization's "The Digital Soil Map of the World" provides a robust foundation for targeted land use strategies and flood mitigation measures. In (Fig.13b), the reclassification of soil types in the study area is depicted, assigning them to the second category, known for its low sensitivity to floods. Assigning weights to soil types, following methodology of Senanayake et al. (2016), enhances flood risk modelling precision.

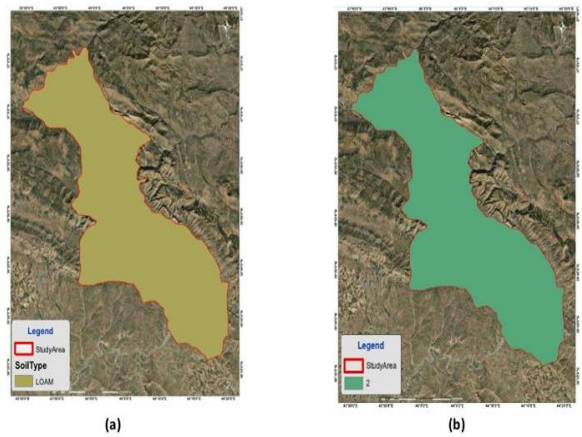

Fig. (13): Thematic map of the soil parameter in the study area

3.2 Interpolation of maps (flood hazard map)

The proposed methodology incorporates the chosen parameters in a linear fashion, taking into account their respective weights. This involves overlaying thematic maps from Figs (3b to 13b) with varying weights within a GIS environment. The outcome is the generation of a flood hazard map (Fig. 14), which categorizes flood vulnerability into five classes: very low, low, moderate, high, and very high.

Examining the flood hazard map (Fig. 14), it is evident that regions characterized by very high and high levels of susceptibility to floods are concentrated in the central, southeastern, southwestern, and a limited area in the northwest of the study area. The distribution of the study area across different levels of flood susceptibility is as follows (Fig. 15): 14% falls into the very high class, 24% into the high class, 23% into the moderate class, 25% into the low class, and 14% into the very low class. Very high flood vulnerability areas are close to rivers especially the Greater Zab and Rezan rivers. Very high flood vulnerability areas are close to rivers especially the Greater Zab and Rezan rivers.

Fig. 16's pie charts depict land use distribution in flood-prone zones in the study area. Pastures and agriculture dominate the landscape, alongside varying urbanization and natural features. Very high-risk areas are mainly grasslands (69%), extensive agriculture (19%), and urban areas (7%). In "High-risk" zones, urban presence increases to 6%. "Low" risk areas are mostly pasturing (95%), with minimal urban and agricultural land. "Very low" risk areas are predominantly grassland (95%), with more trees (5%) and no urban areas. "Moderate" risk areas are primarily pastoral land (92 %) with a mix of urban (3%) and agricultural land (2%). This analysis highlights the need for integrating land management and flood mitigation strategies. According to the flood susceptibility category, the villages in the area under investigation are classified in the Table 7 below.

Table (7): Villages classification according to flood hazard susceptibility in the study area

#	Flood Severity Level	No. of Villages	Villages Names
1	Very Low	9	Bekrse, Dawidka, Dawudka, Harbu, Rekul, Rishma, Sita, Turshke, Sare Pirsurnd
2	Low	17	Alka, Avadur, Babsefa, Bazi Gali, Bekhma Dam Compound, Hizan, Kulka, Mande, Merake, Nadar, Saka, Saluka, Sefiya, Shine, Shinkil, Tuizhge, Zewa
3	Moderate	29	Aliyan, Amokan, Baze, Bekhma Lower, Bekhma Upper, Darbutk, Hamdula, Harine, Hasnaka New, Hasne, Hostan, Irwan, Isumara, Marane, Merge, Naqabe, Presa, Qalatuk, Rezan, Safte, Sako Lower, Sarkandal, Savra, Shanik, Shekhan, Sinawah, Susnawa, Taylli, Teli
4	High	43	Amada Upper, Asta, Babana, Balinda, Bardin, Baruzh Zawa, Barzan, Bibana, Birakapra, Biye, Dinarta, Dola Tesu, Ekmale, Galuk Mam Sak Lower, Goraz,Harbo, Hardan, Harwe, Havndka, Hasnaka Old, Kampe, Khalan, Kuna Sikhur, Merake, Mala Musa, Mlane, Nerwa, Qalata, Qasrok, Resha, Safte, Sarkavr, Sarke, Sarokani, Sawa, Shiva Guiske, Sinawa, Sreshma, Surya, Suse, Warya, Zinta, Zuragvan
5	Very High	36	Amada Lower, Ashkawta, Avdalan, Bekhme, Bekres, Birakapra, Ble, Busel, Cham Beke, Denava, Galava, Galuk Mam Sak Upper, Havinka, Kalati, Kampa Ashghale, Kani Chirgan, Kani Dir, Kani Halan, Mafraq Dinarta, Malman, Malojan, Merge, Raziyan, Rezan, Sar Gali, Sarbardok, Shanadar, Shanik, Shre, Soran Lower, Turishk, Usta, Zebar, Zewa Lower, Zewa Upper, Zhirka

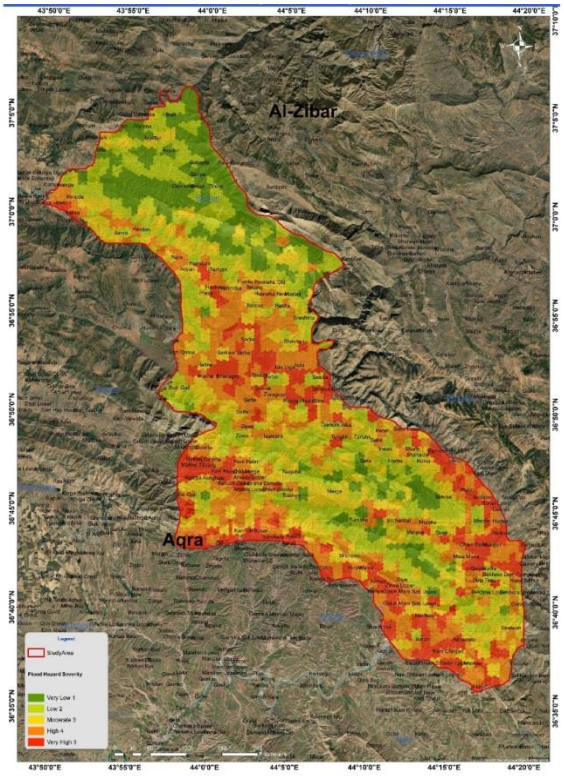

Fig. (14): Flood hazard map: (FHI index)

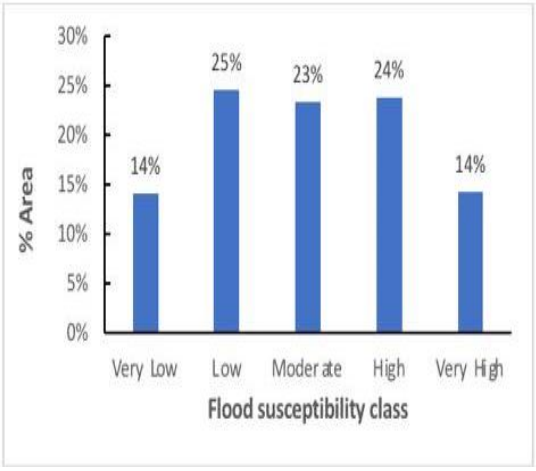

Fig. (15): Distribution of the study area across different classes of flood susceptibility

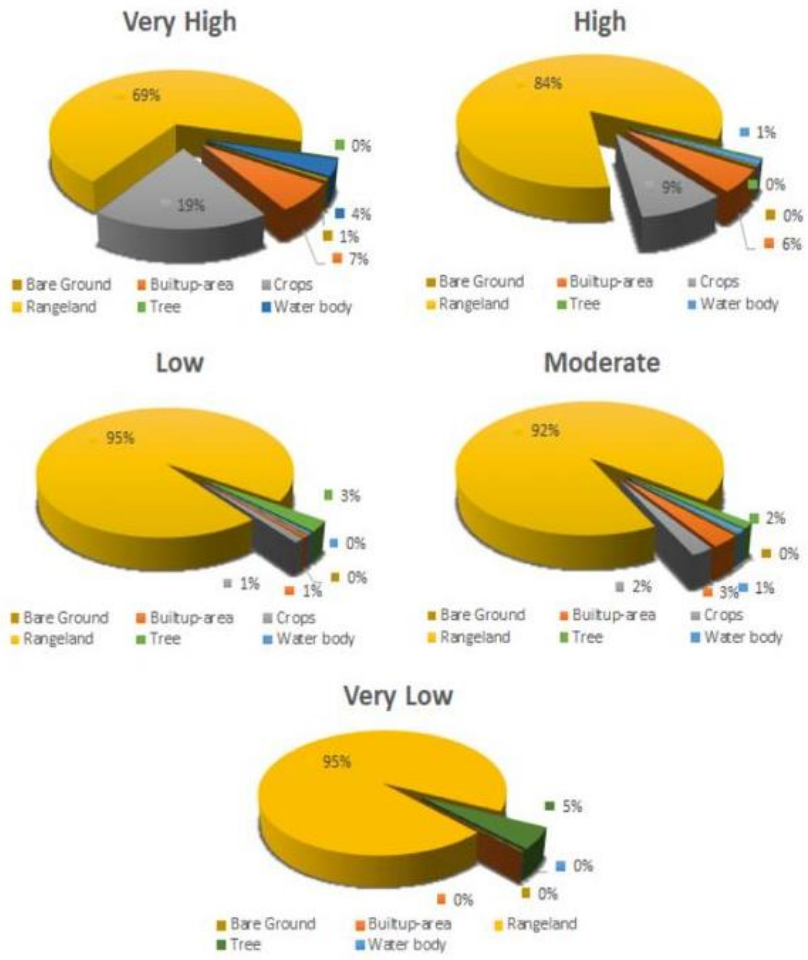

Fig. (16): Distribution of land use in flood hazard areas

3.3 Verification – Sensitivity Analysis:

The observed historical flood map for three years (2020,2022, and 2023) were compared with the final flood susceptibility (hazard) map created in this study using the AHP-GIS/RS technique. Employing the "Map Query" operation, the flooded area was cross-referenced with the regions identified as very high and high flood susceptibility classes on the map (Fig. 17). The resulting map indicated significant flooding in areas categorized as having a very high and high predisposition to floods.

Through an analysis of historical flood data projected onto the flood risk map, the total area exposed to flooding within the study area is (257 km^2), accounting for the entire study area where floods occurred during the three years (2020, 2021, and 2022). Numerous cases were identified in different regions, and these areas were distributed on the flood map generated in this investigation, as detailed in Table 8: (66.14 km^2) in areas highly susceptible to floods. Additionally, (79.43 km^2) was pinpointed in highly vulnerable areas, (53.19 km^2) in regions classified as moderately flood-prone, and (39.93 km^2) and (18.18 km^2) in low and very low-lying flood-prone areas, respectively. highlighting the reliability of the susceptibility map. This underscores its utility as an effective early warning system for potential flood events.

Table (8): Areas according to the flood susceptibility class and historical flood observation locations

Flood Hazard Classes	flood susceptibility (hazard) map		Historical flood occurrence observations			
	Area (km^2)	% Area	Area (km^2)	% Area	% Area of flood compare to hazard map area	% of each severity class
Very high	126.9	14	66.2	26	52	38
High	217.6	24	79.5	31	37	27
Moderate	208.5	23	53.2	21	25.5	19
Low	226.6	25	39.9	15	18	13
Very Low	126.9	14	18.8	7	6	4
Total Area	906.5		257.6			

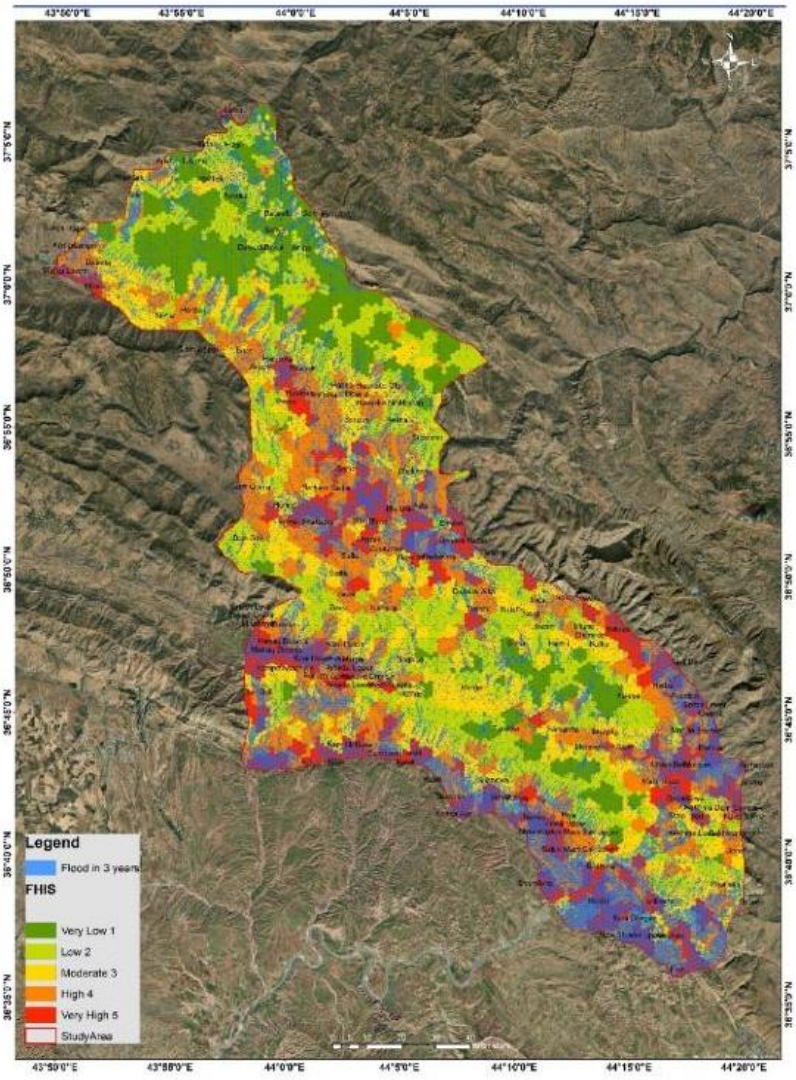

Fig. (17): The sensitivity analysis by comparing the observed historical flood map for three years (2020,2022, and 2023) with the final flood hazard map created in the study area

4 Conclusions:

Formulating a framework for classifying flood-prone areas in the Bazan area, is the main analytical aim of this research. This is significant for informed decision-making as it provides a roadmap for implementing necessary flood mitigation measures. The established methodology. The established methodology utilizes the FHI index to spatially analyze ten parameters: Topographic Wetness Index,

Elevation, Slope, Precipitation, (LULC), (NDVI), Distance from River, Distance from Road, Drainage Density, and Soil Type.

To ascertain the relation significance of each factor, a sophisticated numerical method, the Analytic Hierarchy Process, was conducted. The topographic Wetness Index received a higher weight, while soil type was assigned a lower weight.

Subsequently, the impact of each criterion was combined linearly, and their numerical superimposition ensued in a mapped conception of highly prone areas.

The resulted flood hazard map in terms of natural and anthropogenic factors were categorized into five major modules with flood potentiality from low to very high. Correspondingly, and discovered that an area of 344.5 km^2 (38%) was determined in very high flood and high flood susceptibility zones that were in the vicinity of rivers, whereas an area of 208.5 km^2 (23%) had moderate and 353.5km^2 (39%) had low and very low flood susceptibility. Additionally, the villages and built-up areas in the study area were categorized into different flood classes ranging from very high to very low. Among these classifications, 79 villages were classified within the very high and high flood risk categories.

This investigation validated the generated flood-hazard map by comparing it with historical flood events at previously flooded locations. The outcomes demonstrated the reliability and outstanding predictive capability of the derived flood-hazard map.

The ten parameters used help assess the risk to housing, infrastructure and agricultural production, thereby supporting preparedness and risk reduction for displacement and damage to property and livelihoods. The parameters used in this investigation would also suggest a basis for identifying locations where specific types of Nature-based Solutions (NBS) could be used to optimum effect to reduce flood risk by reducing the rate of runoff and increasing infiltration. The investigation therefore provides a method of better risk reduction through comprehensive and systematic large-scale flood hazard evaluation. The method's parameters also suggest the opportunity for an evidence-driven foundation to overcome one of the main challenges of NBS: the high cost of designing low-cost NBS infrastructure on a large geographic scale could be reduced by high-resolution analysis of topography, soil permeability, water retention, vegetation and land use.

5 Recommendations:

This study can be replicated in other areas or contexts if key conditions are met. First, local authorities must support the approach and acknowledge that the process of developing flood hazard maps is just as important as the maps themselves. Second, adequate technical and human resources are required, as the model demands expertise in GIS software. With the current progress in information technology (IT) and e-governance across the Iraqi Kurdistan region, likely, that many local governorates will soon be able to implement the GIS flood hazard mapping model.

References:

ALI, B. A. & MAWLOOD, D. K. 2023a. Applying the SWMM Software Model for the High Potential Flood-Risk Zone for Limited Catchments in Erbil City Governorate. *Zanco Journal of Pure and Applied Sciences,* 35**,** 41-50.

ALI, B. A. & MAWLOOD, D. K. 2023b. Urban Flood Simulation in Erbil City by Using Storm Water Management Model (SWMM). *Zanco Journal of Pure and Applied Sciences,* 35**,** 1-11.

ALTHUWAYNEE, O. F., PRADHAN, B., PARK, H.-J. & LEE, J. H. 2014. A novel ensemble bivariate statistical evidential belief function with knowledge-based analytical hierarchy process and multivariate statistical logistic regression for landslide susceptibility mapping. *Catena,* 114**,** 21-36.

ARCGIS. 2010. *ArcGIS* [Online]. Available: https://www.esri.com [Accessed 2024].

CHORLEY, R. J. & KENNEDY, B. A. 1971. *Physical geography: a systems approach*, Prentice Hall.

CORREIA, F. N., DA GRAÇA SARAIVA, M., DA SILVA, F. N. & RAMOS, I. 1999. Floodplain management in urban developing areas. Part I. Urban growth scenarios and land-use controls. *Water resources management,* 13**,** 1-21.

ELKHRACHY, I. 2015. Flash flood hazard mapping using satellite images and GIS tools: a case study of Najran City, Kingdom of Saudi Arabia (KSA). *The Egyptian Journal of Remote Sensing and Space Science,* 18**,** 261-278.

FARR, T. G., ROSEN, P. A., CARO, E., CRIPPEN, R., DUREN, R., HENSLEY, S., KOBRICK, M., PALLER, M., RODRIGUEZ, E. & ROTH, L. 2007. The shuttle radar topography mission. *Reviews of geophysics,* 45.

GHANBARPOUR, M., SALIMI, S. & HIPEL, K. 2013. A comparative evaluation of flood mitigation alternatives using GIS-based river hydraulics modelling and multicriteria decision analysis. *Journal of Flood Risk Management,* 6**,** 319-331.

GIGOVIĆ, L., PAMUČAR, D., BAJIĆ, Z. & DROBNJAK, S. 2017. Application of GIS-interval rough AHP methodology for flood hazard mapping in urban areas. *Water,* 9**,** 360.

GREEN, C. H., PARKER, D. J. & TUNSTALL, S. M. 2000. Assessment of flood control and management options. *WCD Thematic reviews. World Commission on Dams Secretariat, South Africa*.

HAMMAMI, S., ZOUHRI, L., SOUISSI, D., SOUEI, A., ZGHIBI, A., MARZOUGUI, A. & DLALA, M. 2019. Application of the GIS based multi-criteria decision analysis and analytical hierarchy process (AHP) in the flood susceptibility mapping (Tunisia). *Arabian Journal of Geosciences,* 12**,** 1-16.

HANDBOOK, S. U. & TOOLS, E. 2015. Sentinel-2 user handbook. *ESA Standard Document Date,* 1**,** 1-64.

HANRATTY, P. & JOSEPH, B. 1992. Decision-making in chemical engineering and expert systems: application of the analytic hierarchy process to reactor selection. *Computers & chemical engineering,* 16**,** 849-860.

KALIRAJ, S., CHANDRASEKAR, N. & MAGESH, N. 2014. Identification of potential groundwater recharge zones in Vaigai upper basin, Tamil Nadu, using GIS-based analytical hierarchical process (AHP) technique. *Arabian Journal of Geosciences,* 7**,** 1385-1401.

KAZAKIS, N., KOUGIAS, I. & PATSIALIS, T. 2015. Assessment of flood hazard areas at a regional scale using an index-based approach and Analytical Hierarchy Process: Application in Rhodope–Evros region, Greece. *Science of the Total Environment,* 538**,** 555-563.

LAWAL, D. U., YUSOF, K. W., HASHIM, M. A. & BALOGUN, A.-L. Spatial analytic hierarchy process model for flood forecasting: An integrated approach. IOP conference series: Earth and environmental science, 2014. IOP Publishing, 012029.

LIU, Y. B., GEBREMESKEL, S., DE SMEDT, F., HOFFMANN, L. & PFISTER, L. 2003. A diffusive transport approach for flow routing in GIS-based flood modeling. *Journal of Hydrology,* 283**,** 91-106.

MALCZEWSKI, J. 2006. GIS-based multicriteria decision analysis: a survey of the literature. *International journal of geographical information science,* 20**,** 703-726.

MOORE, I. D., GRAYSON, R. & LADSON, A. 1991. Digital terrain modelling: a review of hydrological, geomorphological, and biological applications. *Hydrological processes,* 5**,** 3-30.

MUHAMMAD, S. H., ABO, A. A. & AZEEZ, Y. W. 2023. Estimation of Flood Hydrograph for Aquban Catchment Area Using Two Models. *Zanco Journal of Pure and Applied Sciences,* 35**,** 59-66.

NATURE_IRAQ. 2007. *Barzan Area (E8)* [Online]. Available: http://www.natureiraq.org/uploads/9/2/7/0/9270858/barzan_area-e8.pdf [Accessed 2024].

NATURE_IRAQ 2007, 2009. Barzan area & Gali Balnda (iq004).

OKORAFOR, O. O., CHIKWUE, M. I., NWAKUBA, N. R. & NWAOBI, F. A. 2021. Mapping of flood prone areas in Imo State, Southeastern Nigeria using GIS techniques. *Scientific Research Journal,* 9**,** 1-9.

PIRDASHTI, M., GHADI, A., MOHAMMADI, M. & SHOJATALAB, G. 2009. Multi-criteria decision-making selection model with application to chemical engineering management decisions. *International Journal of Chemical and Molecular Engineering,* 3**,** 1-6.

POUSSIN, J. K., BOTZEN, W. W. & AERTS, J. C. 2014. Factors of influence on flood damage mitigation behaviour by households. *Environmental Science & Policy,* 40**,** 69-77.

RAHMATI, O., ZEINIVAND, H. & BESHARAT, M. 2016. Flood hazard zoning in Yasooj region, Iran, using GIS and multi-criteria decision analysis. *Geomatics, Natural Hazards and Risk,* 7**,** 1000-1017.

RAZANDI, Y., POURGHASEMI, H. R., NEISANI, N. S. & RAHMATI, O. 2015. Application of analytical hierarchy process, frequency ratio, and certainty factor models for groundwater potential mapping using GIS. *Earth Science Informatics,* 8**,** 867-883.

ROUSE, J. W., HAAS, R. H., SCHELL, J. A. & DEERING, D. W. 1974. Monitoring vegetation systems in the Great Plains with ERTS. *NASA Spec. Publ,* 351**,** 309.

SAATY, T. L. 1977. A scaling method for priorities in hierarchical structures. *Journal of mathematical psychology,* 15**,** 234-281.

SAATY, T. L., VARGAS, L. G., SAATY, T. L. & VARGAS, L. G. 2012. The seven pillars of the analytic hierarchy process. *Models, methods, concepts & applications of the analytic hierarchy process***,** 23-40.

SENANAYAKE, I., DISSANAYAKE, D., MAYADUNNA, B. & WEERASEKERA, W. 2016. An approach to delineate groundwater recharge potential sites in Ambalantota, Sri Lanka using GIS techniques. *Geoscience Frontiers,* 7**,** 115-124.

SIDDAYAO, G. P., VALDEZ, S. E. & FERNANDEZ, P. L. 2014. Analytic hierarchy process (AHP) in spatial modeling for floodplain risk assessment. *International Journal of Machine Learning and Computing,* 4**,** 450.

SWAIN, K. C., SINGHA, C. & NAYAK, L. 2020. Flood susceptibility mapping through the GIS-AHP technique using the cloud. *ISPRS International Journal of Geo-Information,* 9**,** 720.

USHIYAMA, T., KWAK, Y., LEDVINKA, O., IWAMI, Y. & DANHELKA, J. Interdisciplinary approach for assessment of continental river flood risk: a case study of the Czech Republic. EGU General Assembly Conference Abstracts, 2017. 5737.

WANG, X. & XIE, H. 2018. A review on applications of remote sensing and geographic information systems (GIS) in water resources and flood risk management. *Water,* 10**,** 608.

WANG, Y., LI, Z., TANG, Z. & ZENG, G. 2011. A GIS-based spatial multi-criteria approach for flood risk assessment in the Dongting Lake Region, Hunan, Central China. *Water resources management,* 25**,** 3465-3484.

YAHAYA, S. Multi criteria analysis for flood vulnerable areas in Hadejia-Jama'Area river basin. Nigeria ASPRS Annual conference Portland, 2008.

YANG, M., QIAN, X., ZHANG, Y., SHENG, J., SHEN, D. & GE, Y. 2011. Spatial multicriteria decision analysis of flood risks in aging-dam management in China: A framework and case study. *International journal of environmental research and public health,* 8**,** 1368-1387.